J. Fluid Mech. (1994), *vol.* 274, *pp.* 197–217

Dynamics of a drop in a constricted capillary tube

By T. M. TSAI AND MICHAEL J. MIKSIS

Department of Engineering Sciences and Applied Mathematics, Northwestern University, Evanston, IL 60208, USA

(Received 24 September 1993 and in revised form 15 February 1994)

Here we study the dynamics of a bubble or drop as it is driven by a pressure gradient through a capillary tube. For the case of a straight capillary, the drop can either approach a steady-state shape or the rear of the drop develops a re-entrant cavity. Also, depending on the initial conditions, the drop can break apart into smaller drops. For flow through a constricted capillary tube, depending on the physical parameters of the problem, the drop can either move through the constriction or break into two or more pieces as it moves past the constriction. We study this snap-off process numerically and determine the effect of the physical parameters on the dynamics of the drop.

1. Introduction

Foam flow in porous media has attracted considerable interest recently because of its applications to enhanced oil recovery and hazardous waste management. These foams have been shown to reduce the gas mobility, and therefore reduce gravity override and channelling which would otherwise lead to premature gas breakthrough. Hence using foams as a means of sweeping out a given porous material of either oil or another liquid appears to be a very promising process. The fundamental mechanism associated with the formation of a foam in porous media is called snap-off. This process was identified by Roof (1970) as the primary mechanism in the breakup of a droplet (or bubble) as it travels through a porous medium. In particular, as a droplet of one liquid passes through a constriction in its path, the capillary pressure at the nose of the droplet is less than the capillary pressure at the neck of the constriction. This pressure difference will initiate an instability along the interface which splits the droplet into two. Since the texture, effective viscosity and other macroscopic properties of the foam depend on the size of bubbles being generated, it is of practical interest to understand the breakup of a gas bubble in a porous medium. In this study we use straight and constricted capillaries as a simplified model for a pore geometry. Our goal is to present a numerical study of the deformation and breakup of a drop as it travels through the capillary tube due to an imposed pressure gradient.

Under the assumption of creeping flow, the axisymmetric motion of a neutrally buoyant drop or bubble moving through a straight or constricted circular capillary is investigated. We will assume that the suspending fluid has viscosity μ while the drop has a viscosity $\lambda\mu$. Hence λ is the viscosity ratio and we will find that the dynamics of the drop will depend on λ. The limit of $\lambda = 0$ or λ small can be considered as the case of a bubble. Therefore, our results are applicable to either a drop or bubble, depending on λ and we will use the words bubble or drop interchangeably with the specific meaning depending on the value of λ. The problem is solved numerically by using a boundary integral method. This numerical method has been used by many researchers and is proven to be effective in solving free boundary problems. For example,

Youngren & Acrivos (1976) and Rallison & Acrivos (1978) studied the deformation of a gas bubble and viscous drop in an extensional flow; Lee & Leal (1982) and Chi & Leal (1989) considered a solid sphere and a viscous drop moving toward a fluid interface.

The motion of a drop or bubble in a capillary tube has been studied by others. For example, Martinez & Udell (1990) computed the steady-state solutions of a neutrally buoyant axisymmetric drop through a straight capillary. The drop size in their studies, defined to be the ratio of undeformed drop radius a_0 to the radius of the tube R_0, is between 0.5 and 1.15. Their results agree well with the experiments carried out by Ho & Leal (1975). They also reported a re-entrant cavity at the back of a steady-shape drop for capillary number, $Ca = \mu V/\gamma$, around 0.75 and $a_0/R_0 = 0.726$. Here μ is the viscosity, V is the average bulk velocity of the suspending fluid and γ is the constant interfacial surface tension. In this study, we compute the transient motion of a drop in both a straight and a constricted capillary tube. Depending on the initial conditions and the capillary number, we find that the drop can either approach a steady shape, break up into smaller drops or have a jet of suspending fluid penetrate from the back. Thus our computations in the straight capillary case not only verify the previous results on the steady-state behaviour of a drop but also allow us to consider values of the capillary number where only unsteady solutions are found to exist. Recently, Olbricht & Kung (1992) carried out an extensive experimental study for the motion of drops in a straight capillary. They considered capillary numbers from 0.05 to greater than 4 and determined the critical value that leads to drop breakup for a wide range of drop sizes and viscosity ratios. Our computations show a close resemblance to the dynamic behaviour of the drops in these experiments. Also, recently, Borhan & Mao (1992) extended the solutions of Martinez & Udell (1990) to include the presence of surfactants. In a related work Pozrikidis (1992) studied the periodic motion of a train of viscous drops settling or rising due to buoyancy in a straight capillary tube.

There has been extensive work on the motion of a semi-infinite bubble in a straight capillary tube. For example, Bretherton (1961) used lubrication theory to study the steady translation of an inviscid bubble for $a_0/R_0 \gg 1$ and $Ca \to 0$. His results show that there is a thin film with constant thickness between the bubble and the tube wall, and the thickness of the film is a function of Ca. Bretherton also carried out experiments to check the theory and found that the theory underpredicts the measured values of film thickness as Ca becomes small. Similar conclusions are reported from the experimental investigations of Schwartz, Princen & Kiss (1986). Reinelt & Saffman (1985) used finite difference methods and Shen & Udell (1985) used finite element methods to compute the leading meniscus of a semi-infinite bubble. Martinez & Udell (1989) computed both leading and trailing menisci of a large bubble using the boundary integral method.

For $a_0/R_0 \ll 1$, Hetsroni, Haber & Wacholder (1970) used the method of reflections to solve for the flow fields in and around a single spherical drop in a capillary tube. Upon substituting the velocity fields in the normal stress balance, they also obtained the leading-order correction for the deformed drop shape provided $Ca \to 0$. Brenner (1971) obtained the extra pressure loss due to the presence of the drop using the reciprocal theorem for low-Reynolds-number flow. Brenner's results indicate that the value of extra pressure loss can be either positive or negative depending on the magnitude of viscosity ratio λ.

For the flow of a drop or bubble through a constricted capillary, Goldsmith & Mason (1963) connected two capillaries of radius 0.1 cm and 0.4 cm to form half of a constriction. They observed a series of bubbles being generated near the entry of the smaller capillary when a large single bubble was driven into the smaller capillary from

the large one. Roof (1970) analysed the static capillary pressure difference across an oil–water interface and found that, for a given radius of constriction, there is an equilibrium position of the leading meniscus of the interface beyond which snap-off will occur if water can flow into the constriction. His experiments confirm the results but a groove must be cut axially along the constriction to form a channel for water to flow into the constriction. Otherwise, no snap-off was observed even when the drop front passes the predicted equilibrium position and the flow of suspending fluid was stopped. He then observed that the drop maintains its shape and position for hours. Olbricht & Leal (1983) also found snap-off of a gas bubble at the first constriction in a periodically constricted capillary tube in their experimental study. Martinez & Udell (1988) studied numerically the motion of a drop through a periodically constricted tube but did not observe snap-off. For the case of $a_0/R_0 \gg 1$, Shen (1984) used lubrication theory and finite difference methods to compute the growth of a liquid collar at the constriction. Although the results indicate that the collar is growing in time, no snap-off was observed numerically. Gauglitz, St. Laurent & Radke (1988) determined the breakup time and the generated bubble length experimentally for the flow of a large bubble in a constricted capillary. Combining Bretherton's results for the film thickness and the analysis of Hammond (1983) for the thin film instability, they found that the breakup time is inversely proportional to the square of the bubble capillary number Ca_T while the generated bubble length is inversely proportional to Ca_T. Their bubble capillary number Ca_T is defined as $\mu V_b/\gamma$, where V_b is the steady velocity of the bubble in the straight section of the tube. The experimental results on the breakup time and generated bubble length agree very well with the theoretical predictions. Gauglitz & Radke (1990) derived a small-slope evolution equation for the thickness of a thin film in a constricted capillary which retains the essence of the curvature terms in a cylindrical geometry. They solved the evolution equation by finite element methods and showed that the liquid film grows in time at the neck of the constriction and snaps off a new bubble. Using a boundary integral method, we solve the Stokes equations with the complete boundary conditions and show the dependence of the snap-off mechanism on the initial drop configuration, drop size, capillary number and viscosity ratio.

We begin with a formulation of the equations of motion in §2. Then in §3 we describe the numerical method and discuss the accuracy and convergence of the numerical scheme. The dynamics of the drop is dependent on the initial conditions and is discussed in §4. The dynamics of the drop in a straight capillary are discussed in §5 and in §6 we discuss the results for the constricted capillary tube.

2. Formulation

We consider the axisymmetric flow of a drop or bubble in a capillary tube as shown in figure 1. A cylindrical coordinate system is employed with the z-axis parallel to the centreline of the capillary tube. The drop, $\boldsymbol{\Omega}_d$, is assumed to be neutrally buoyant so the effects of gravity are neglected. The volume of the drop is $\frac{4}{3}\pi a_0^3$, where a_0 is its undeformed radius. The suspending fluid in Ω is driven by an imposed pressure gradient and flows at a constant volume flux Q. The Reynolds number is assumed to be small so the system is in a state of creeping motion.

The governing equations for the suspending fluid are conservation of mass and momentum:

$$\nabla \cdot \boldsymbol{v} = 0, \tag{2.1}$$

$$\nabla \cdot \boldsymbol{\sigma}(\boldsymbol{v}) = \mathbf{0}, \tag{2.2}$$

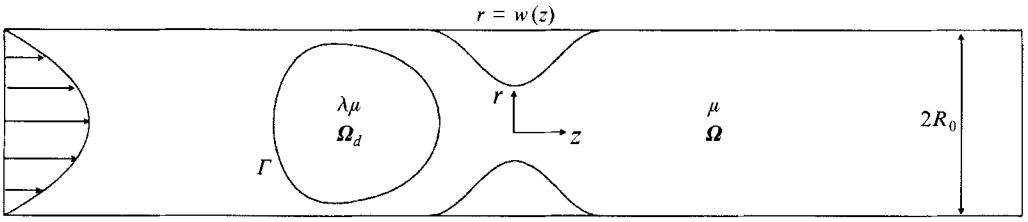

FIGURE 1. A bubble in a constricted capillary tube.

for $x \in \Omega$, where $\sigma(v) = -pI + \mu\{\nabla v + (\nabla v)^T\}$, v is the velocity field, p is the pressure, and μ is the viscosity of the suspending fluid. Similarly for the drop where $x \in \Omega_d$, we have

$$\nabla \cdot u = 0, \tag{2.3}$$

$$\nabla \cdot \sigma(u) = 0, \tag{2.4}$$

where $\sigma(u) = -p_d I + \lambda\mu\{\nabla u + (\nabla u)^T\}$ and u is the velocity field, p_d is the pressure, and $\lambda\mu$ is the viscosity of the drop.

The boundary condition along the tube wall is no slip:

$$v = 0. \tag{2.5}$$

Along the interface between the drop and the suspending fluid, Γ, the boundary conditions are the continuity of velocity

$$u = v, \tag{2.6}$$

the stress balance condition

$$\sigma(v) \cdot n - \sigma(u) \cdot n = \gamma(\nabla \cdot n) n, \tag{2.7}$$

and the kinematic condition

$$\frac{\partial Y}{\partial t}(x, t) \cdot n = v \cdot n, \tag{2.8}$$

where γ is the constant interfacial surface tension, n is the unit normal vector pointing away from the suspending fluid, and Y is the position vector on Γ. Three conditions are necessary on Γ since the interface is a free surface and has to be determined together with the velocity and pressure fields. Finally, we require that the velocity of the suspending fluid approaches Poiseuille flow far ahead of and behind the drop and the constriction, i.e. as $|z| \to \infty$,

$$v = \frac{2Q}{\pi R_0^4}(R_0^2 - r^2) e_z, \tag{2.9}$$

where Q is the constant volume flux and e_z is the unit vector along the axis of the cylindrical tube.

The governing equations and boundary conditions can be non-dimensionalized. Select R_0, the radius of the straight section of the tube, as the lengthscale; $V = Q/\pi R_0^2$, which is the average velocity of the suspending fluid, as the velocity scale; $\mu V/R_0$ as the unit of pressure and R_0/V as the unit of time. The dimensionless boundary conditions along the tube wall are

$$v = 0 \quad \text{at} \quad r = w(z), \quad -\infty < z < \infty, \tag{2.10}$$

where $r = w(z)$ describes the geometry of the tube wall. At the free surface Γ, the conditions are

$$\boldsymbol{u} = \boldsymbol{v}, \tag{2.11}$$

$$\boldsymbol{\sigma}(\boldsymbol{v})\cdot\boldsymbol{n} - \boldsymbol{\sigma}(\boldsymbol{u})\cdot\boldsymbol{n} = \frac{1}{Ca}(\nabla\cdot\boldsymbol{n})\,\boldsymbol{n}, \tag{2.12}$$

$$\frac{\partial \boldsymbol{Y}}{\partial t}(\boldsymbol{x}, t)\cdot\boldsymbol{n} = \boldsymbol{v}\cdot\boldsymbol{n}. \tag{2.13}$$

Also

$$\boldsymbol{v} = 2(1-r^2)\,\boldsymbol{e}_z \quad \text{for} \quad z\to\pm\infty, \quad 0\leqslant r\leqslant 1 \tag{2.14}$$

at the upstream and downstream boundaries.

Three parameters emerge for the flow of a drop in a straight capillary tube. They are the effective drop radius $a = a_0/R_0$, the viscosity ratio λ and the capillary number $Ca = \mu V/\gamma$. The capillary number is a measure of the relative importance of the viscous force to the surface tension force. Our aim is to determine the evolution of the drop as a function of these three parameters. As we will see, the initial conditions will also influence the dynamics of the drop and must be included in any discussion of the drop behaviour. In addition to these three parameters, the geometry of the capillary must be determined. For a straight-sided capillary tube, $w = 1$ for all values of z. For a constricted capillary tube the function $w(z)$ must be specified. We will use the function

$$r = w(z) = 1.0 - d\{1.0 + \cos(\pi z/l)\} \tag{2.15}$$

for $-l \leqslant z \leqslant l$, and $w = 1$ otherwise. Note that the neck of the constriction is centred at the origin, and $2d$ and $2l$ specify the depth and the length of the constriction, respectively. Gauglitz & Radke (1990) also used (2.15) for the shape of the constriction in their lubrication analysis. Because of the lubrication assumption in their study, they were required to have d/l small. Here we are free to select any value of this ratio.

3. Numerical method

In order to solve the Stokes equations for this moving boundary problem we reformulate the equations of motion into a system of integral-differential equations. Only an outline of the numerical method used to solve these equations is given here. Details can be found in Tsai (1994). The boundary integral equations for the unknown velocities and tractions are derived using the Green's functions for the Stokes equations given by Ladyzhenskaya (1969). The boundary integral equations are (e.g. see Pozrikidis 1992)

$$(1+\lambda)\,C_{ki}\,v_i(\boldsymbol{x}) + (1-\lambda)\int_\Gamma T_{ik}(\boldsymbol{x},\boldsymbol{y})\,v_i(\boldsymbol{y})\,\mathrm{d}\Gamma + \int_{\Gamma_w} T_{ik}(\boldsymbol{x},\boldsymbol{y})\,v_i(\boldsymbol{y})\,\mathrm{d}\Gamma_w$$

$$-\int_{\Gamma_w} U_{ik}(\boldsymbol{x},\boldsymbol{y})\,t_i(\boldsymbol{v}(\boldsymbol{y}))\,\mathrm{d}\Gamma_w = \frac{1}{Ca}\int_\Gamma U_{ik}(\boldsymbol{x},\boldsymbol{y})(\nabla\cdot\boldsymbol{n})\,n_i(\boldsymbol{y})\,\mathrm{d}\Gamma \quad \text{for} \quad \boldsymbol{x}\in\Gamma, \tag{3.1}$$

and

$$C_{ki}\,v_i(\boldsymbol{x}) + (1-\lambda)\int_\Gamma T_{ik}(\boldsymbol{x},\boldsymbol{y})\,v_i(\boldsymbol{y})\,\mathrm{d}\Gamma + \int_{\Gamma_w} T_{ik}(\boldsymbol{x},\boldsymbol{y})\,v_i(\boldsymbol{y})\,\mathrm{d}\Gamma_w$$

$$-\int_{\Gamma_w} U_{ik}(\boldsymbol{x},\boldsymbol{y})\,t_i(\boldsymbol{v}(\boldsymbol{y}))\,\mathrm{d}\Gamma_w = \frac{1}{Ca}\int_\Gamma U_{ik}(\boldsymbol{x},\boldsymbol{y})(\nabla\cdot\boldsymbol{n})\,n_i(\boldsymbol{y})\,\mathrm{d}\Gamma \quad \text{for} \quad \boldsymbol{x}\in\Gamma_w. \tag{3.2}$$

Here C_{ki} is the principal-value tensor and depends on the smoothness of the boundary, n_i is the unit normal along the boundary and the tractions $t_i(\boldsymbol{v}(\boldsymbol{y})) = \sigma_{ik} n_k$. The boundary Γ_w includes the tube wall plus an upstream and a downstream boundary far away from the drop and the constriction. The upstream and downstream boundaries are necessary in order to have a finite domain of integration. Otherwise we need to integrate along the whole tube wall out to infinity. The kernels of the integral equations are

$$U_{ik}(\boldsymbol{x},\boldsymbol{y}) = \frac{-1}{8\pi}\left\{\frac{\delta_{ik}}{|\boldsymbol{x}-\boldsymbol{y}|} + \frac{(x_i-y_i)(x_k-y_k)}{|\boldsymbol{x}-\boldsymbol{y}|^3}\right\},$$

and

$$T_{ik}(\boldsymbol{x},\boldsymbol{y}) = \frac{-3}{4\pi}\frac{(x_i-y_i)(x_j-y_j)(x_k-y_k)}{|\boldsymbol{x}-\boldsymbol{y}|^5} n_j(\boldsymbol{y}).$$

When the motion is axisymmetric, the surface integrals can be reduced to line integrals along the generating curve of the boundary by performing the azimuthal integrations analytically.

Given an initial shape for the drop, the solutions of the integral equations can be determined numerically. This is done by approximating the integral operator by a linear system of equations. We start by subdividing each boundary with a set of boundary nodes. The unknown variables along the boundaries are approximated using quadratic interpolation between every three nodes. To ensure the continuity of the curvatures, cubic spline interpolations for the axial and radial coordinates of the interface as functions of arclength are also used. All the numerical integrations are carried out with a six-point Gauss quadrature. In this way we generate a full coefficient matrix which is solved using Gauss elimination. For a well-posed problem, either velocities or stresses (or some combinations of both) have to be specified along the boundaries. Hence two unknowns need to be determined at each boundary node. We also need to specify a reference pressure at the upstream boundary in order to guarantee a unique solution at the downstream boundary. Special care is also needed for the boundary nodes located at the corner. The kernel $U_{ik}(\boldsymbol{x},\boldsymbol{y})$ has a logarithmic singularity when $\boldsymbol{y} \to \boldsymbol{x}$. This is treated by subtracting the logarithmic behaviour of the singularity from the integrands and reducing the integrands with the logarithm singularity into a regular part which can be computed numerically and a singular part which is evaluated analytically. Once the linear system of equations is solved and the surface velocities are determined, a second-order Runge–Kutta method is used to integrate the kinematic condition in time. This procedure is then iterated in time in order to determine the evolution of a drop through a straight or constricted capillary.

The accuracy of the numerical solutions can be assessed by monitoring the solutions of the integral equations and the changes in the drop volume at each time step. Convergence checks are done by doubling the number of boundary nodes, N, on the drop surface while keeping the ratio $\Delta t/\Delta s$ fixed. They indicate that the scheme is at least second-order accurate. Here Δt is the time step and Δs is the distance between successive grid points along the interface and is proportional to $1/N$. In figure 2 we plot the percentage volume change versus time for the evolution of an initially spherical bubble moving through a constricted capillary with $Ca = 0.1$, $a = 0.9$ and $\lambda = 0.001$. The time evolution of the bubble interface is illustrated in figure 8 and will be discussed later. We find that the error associated with the drop volume increases in time. However, it can be controlled and kept within a desired tolerance over a finite time interval by taking a large enough number of grid points. The changes in drop volume are always within 1% of the original volume throughout the course of the computations.

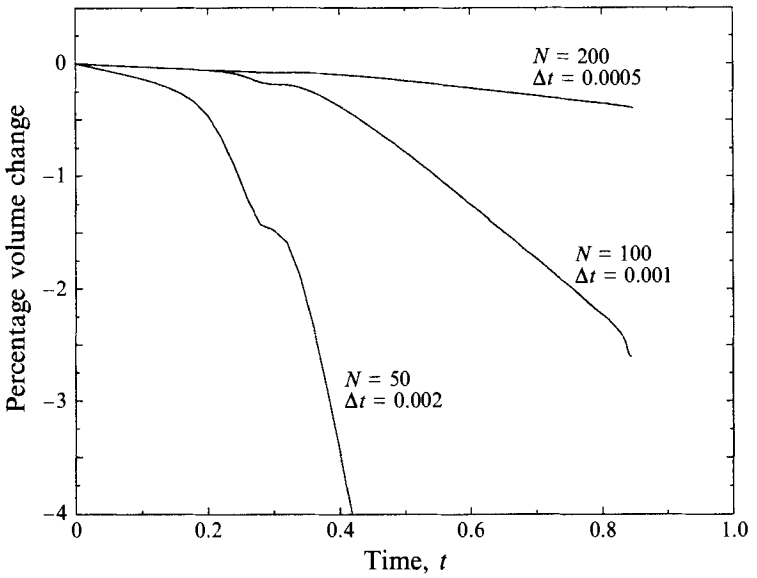

FIGURE 2. Changes in the drop volume versus time.

The upstream and downstream computational boundaries are taken at least R_0 units away from the bubble and the constriction. The position of the upstream and downstream computational boundaries remain fixed in general. However, in the straight capillary the bubble travels a considerable distance and can get close to the downstream boundary. Hence in this case the computation is stopped and restarted with repositioned computational boundaries. The solutions are constantly monitored to ensure that Poiseuille flow is being satisfied at the two ends of our computational boundaries. For the cases presented here, the worst deviation from the parabolic profile was about 1.3% and occurred when the bubble was less than Δt units from snapping off. All computations are performed on the IBM RS6000 and HP9000 workstations with double precision.

4. Initial conditions

In this section, we illustrate the effect of the initial configuration on the dynamics of the drop. In particular, no pressure gradient will be imposed across the capillary tube so that the motion is due only to surface tension. This is achieved with our numerical method by rescaling the equations so that the dependence of Ca in the normal stress condition is shifted to the conditions on the upstream and downstream boundaries. This can be done by selecting a new unit of velocity as γ/μ, pressure as γ/R_0 and time as $R_0\mu/\gamma$. In doing this we can turn off the flow by setting $Ca = 0$ and compute the evolution of the interface driven solely by surface tension. In figure 3 we place two drops of ellipsoid shape with the same volume but different aspect ratios in a capillary tube and let them evolve in time. We set $a = 0.9$ for both drops but in figure 3(a) the aspect ratio is equal to 0.087 while in figure 3(b) we set it equal to 0.038. Depending on the aspect ratio, we see that the drop can either relax back to a spherical shape as in figure 3(a), or as in the case of figure 3(b), break up into three smaller drops. We call the latter behaviour pinch-off: it is driven by surface tension and is due solely to the initial shape of the drop. This pinch-off instability has also been observed in the

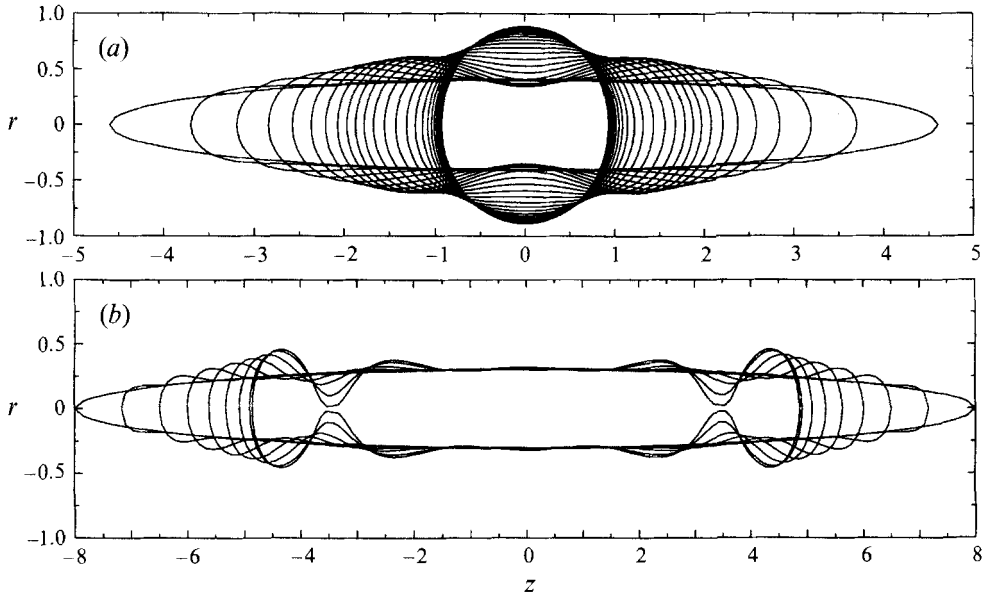

FIGURE 3. Evolution of an initially ellipsoidal drop with $a = 0.9$ and no imposed pressure gradient: (*a*) aspect ratio 0.087; (*b*) aspect ratio 0.038.

computations of E. J. Hinch (1988, personal communication). Hence in choosing the initial data for our flow problem we need to be careful not to excite this instability and confuse it with the snap-off instability. Both instabilities are driven by surface tension but the latter is the result of the bubble moving through the constriction (see e.g. Schwartz *et al.* 1986 for a discussion of the stability of a thin stagnant films). The initial data chosen here will be either a sphere or an ellipsoid for the computations in a straight capillary. In the constricted-tube cases we choose either a sphere or the steady-state shapes determined from the calculations in the straight capillary tube.

5. Straight capillary

We begin the study of the dynamic behaviour of a drop in a capillary tube by considering first the straight capillary. It is important to identify the types of allowable behaviour in this simple geometry before moving on to the constricted capillary tube. Previous numerical studies have determined steady-state drop profiles. Here we solve the initial value problem and are able to determine the unsteady behaviour of a drop in a straight capillary tube as well as its evolution into a steady-state solution when it exists.

The parameters for this problem are the effective radius a, the viscosity ratio λ and the capillary number, Ca. As pointed out in previous studies, Ca plays an important role in determining the existence of steady-state solutions. Typically, for small values of Ca a steady-state profile can be found, but as Ca increases large deformations of the drop shape are expected and the existence of a steady-state solution is not clear. A spherical drop can fit in the tube only for $a < 1$ so one might expect that the behaviour of the drop as a function of a could change in the neighbourhood of 1. This is consistent with the results of Martinez & Udell (1990) who reported that for $a < 0.7$, the drop shapes are insensitive to large variations in Ca and viscosity ratio, while the

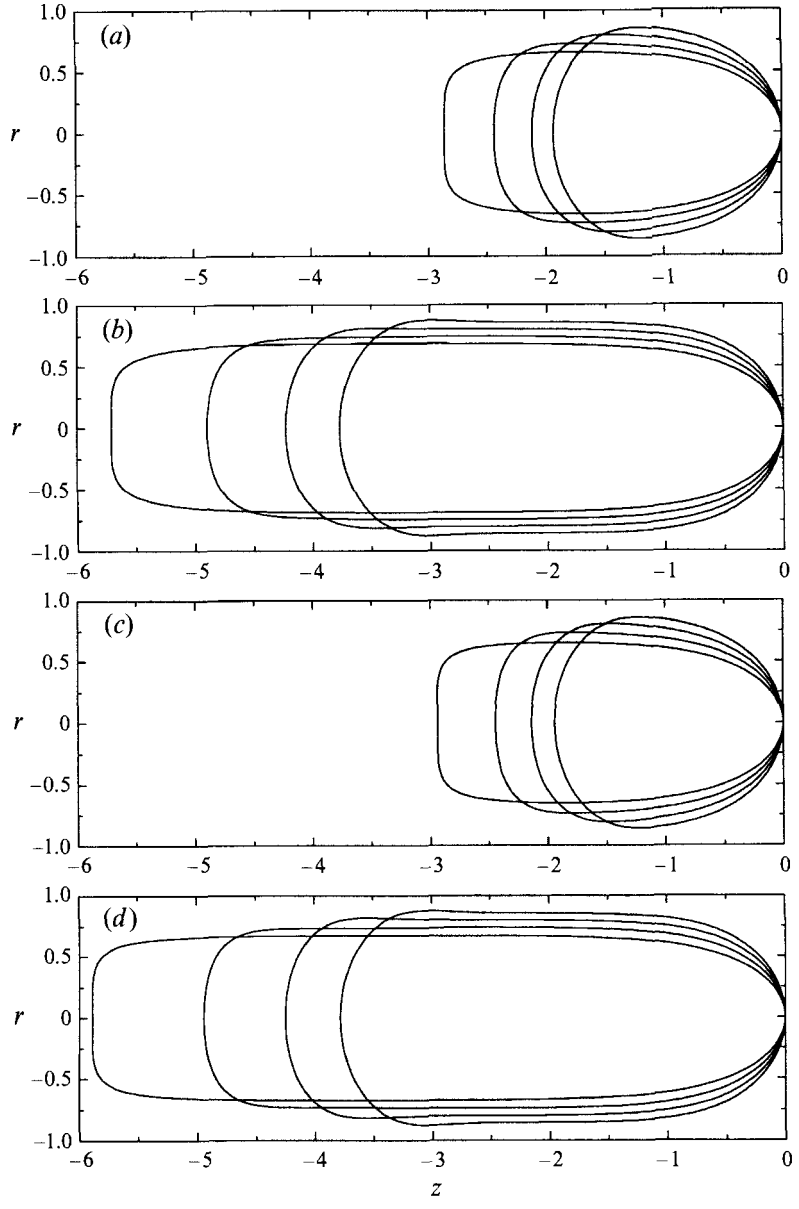

FIGURE 4. Steady drop shape for $Ca = 0.05, 0.1, 0.2, 0.5$ from right to left: (*a*) $a = 0.9$, $\lambda = 0.001$; (*b*) $a = 1.2$, $\lambda = 0.001$; (*c*) $a = 0.9$, $\lambda = 0.1$; (*d*) $a = 1.2$, $\lambda = 0.1$.

computed steady-state solutions for $a \approx 1.1$ show very good agreement with the asymptotic behaviour for $a \gg 1$. In this study we will focus on two drop sizes, $a = 0.9$ and 1.2. We note that a sphere is a possible steady-state solution in the $a = 0.9$ case when there is no flow, hence we might expect some qualitative differences in the transient behaviour for the two cases.

By using our numerical scheme, we can march in time to determine the steady-state solutions of our problem. In figure 4, we plot the steady-state profiles for the effective radii $a = 0.9$ and 1.2, $\lambda = 0.001$ and 0.1, for values of Ca from 0.05 to 0.5. For ease of comparison, the front of each drop is placed at $z = 0$. First note that for $a = 0.9$ the

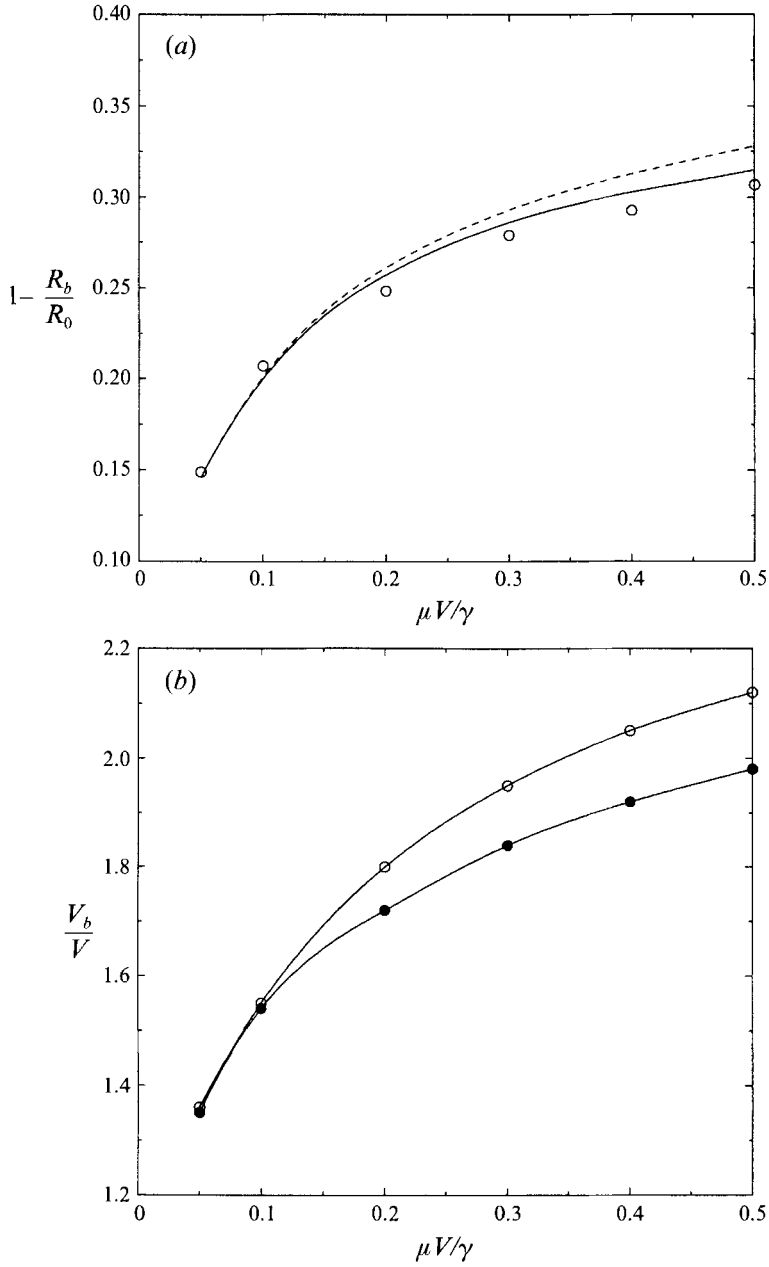

FIGURE 5. (*a*) Film thickness as a function of capillary number; ---, $\lambda = 0.1$; ——, $\lambda = 0.001$; ○, Taylor (1961). (*b*) Steady-state drop velocity as a function of capillary number for $a = 1.2$; ○, $\lambda = 0.001$; ●, $\lambda = 0.1$.

viscosity ratio λ does not appear to have a significant effect on the drop profiles. For $a = 1.2$, we do notice a mild difference in the profiles for the larger values of Ca. In particular, we can see that for $Ca = 0.5$, the $\lambda = 0.1$ drop extends further in the axial direction than the $\lambda = 0.001$ drop. If we were to look carefully, a similar difference occurs for the other capillary numbers. This is consistent with the fact that a more viscous drop will have a stronger resistance to the shearing from the suspending fluid

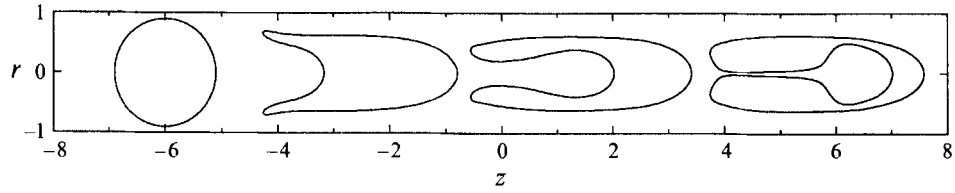

FIGURE 6. Evolution of an initially spherical drop with $a = 0.9$, $\lambda = 0.1$ and $Ca = 1.0$ at $t = 0, 2, 4, 6$.

and hence the overall length is longer in the direction of the imposed flow. A more significant effect on the profiles occurs as we vary the capillary number. Both the overall length and the curvature near the front of the drop increase with Ca while the curvature at the trailing interface decreases. The drop becomes more tapered from the front for larger Ca, which in turn increases the film thickness between the drop and the tube wall. Note that for $a = 1.2$, a film of constant thickness develops near the centre portion of the drop. The thickness of this film depends strongly on Ca but only weakly on λ. In figure 5(*a*) we plot the computed film thickness along with the experimental data from Taylor (1961) taken from his figure 2 where $\lambda \approx 10^{-4}$. We see that the computed film thickness agrees well with the experimental results for $Ca \leqslant 0.1$ but deviates slightly for $Ca \geqslant 0.2$. Figure 5(*a*) also shows that, as λ decreases, the computed film thickness approaches the experimental data as expected. In figure 5(*b*) we plot the steady-state velocity of the bubble, V_b, as a function of Ca. The curves are characteristic of other steady-state calculations, e.g. see Martinez & Udell (1990). We note that the numerical results are for values of Ca larger than those previously appearing in the literature.

As Ca increases, we find that steady-state solutions no longer exist. For large values of Ca our numerical results indicate that the drop undergoes large deformations. For example in figure 6 we compute the transient motions of an initially spherical drop with $a = 0.9$, $\lambda = 0.1$ and $Ca = 1.0$. As time increases, we find that a jet of suspending fluid penetrates into the surface of the drop from the trailing interface. The trailing end of the drop becomes the leading edge of a jet as it travels along the axial axis through the original surface of the drop and leaves a thread of fluid in its path. This behaviour agrees qualitatively well with the experimental investigations of Olbricht & Kung (1992). A time sequence of photographs in their report shows that the leading edge of the jet grows in thickness and becomes varicose before it reaches the front interface of the drop. Similar results were observed by Goldsmith & Mason (1963). These results are also consistent with the steady state calculations of Martinez & Udell (1990) who only find steady-state solutions below a critical value of Ca (this was about 0.75 when $a = 0.726$), hence implying a change in the character of the solutions above the critical Ca.

In figure 6 we see that the leading edge of the jet behaves exactly as observed in the experiments. As time increases, the thread of outer fluid becomes thinner as the end of the tail of the drop folds together. Our computations are terminated when the thread is so thin that it is difficult to resolve numerically. However, it is clear that a compound drop with a large interior of suspending fluid located near the leading front of the original drop is being formed. A critical value of Ca about 2.0 for $a = 0.9$ and $\lambda = 0.1$ was reported by Olbricht & Kung (1992). Our numerical results indicate that $Ca = 1.0$ causes the jetting instability to develop, hence implying that the critical Ca is much lower than the experimental value.

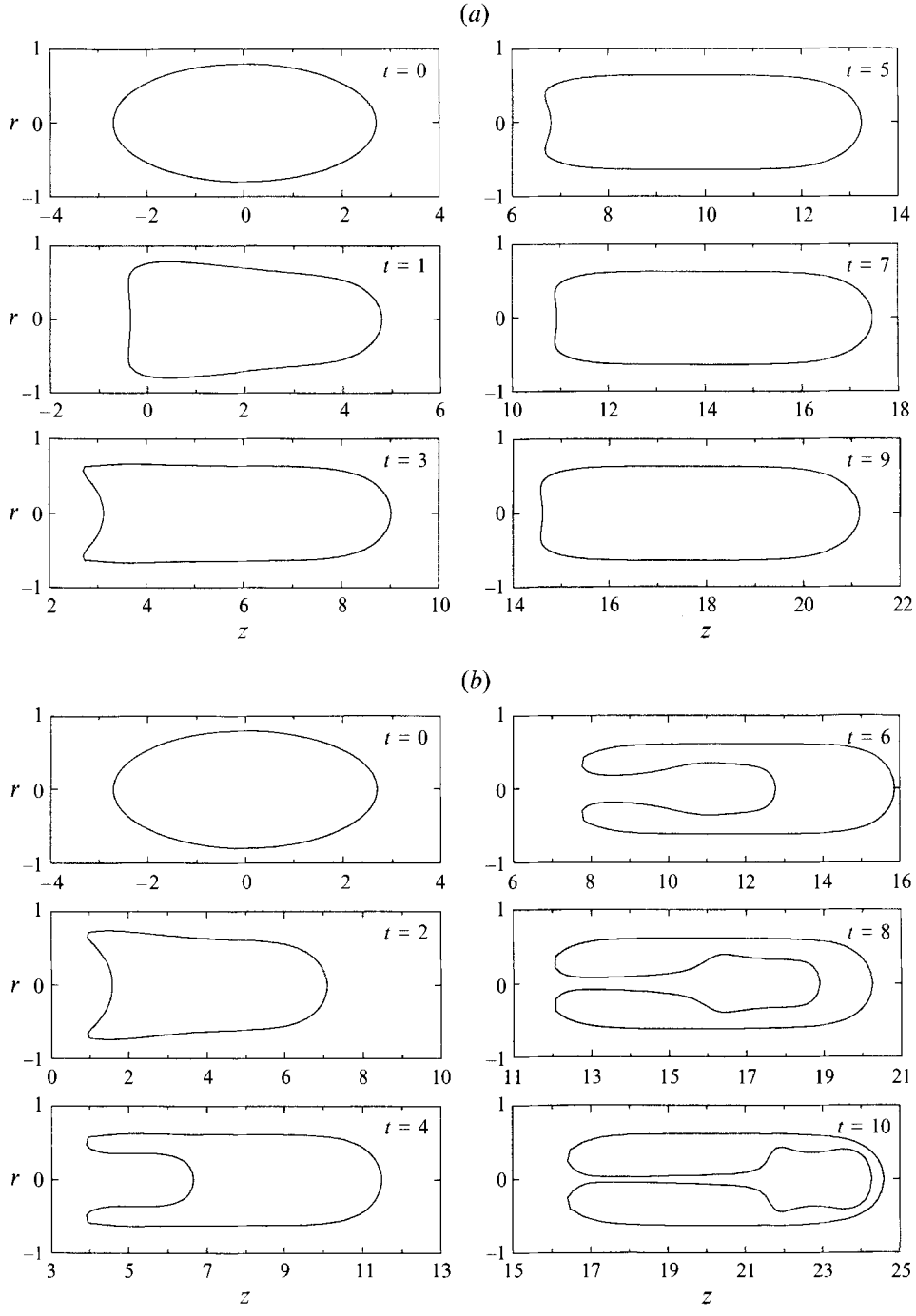

FIGURE 7. Evolution of an initially ellipsoidal drop with $a = 1.2$ and $\lambda = 0.1$: (*a*) $Ca = 1.0$ at $t = 0, 1, 3, 5, 7, 9$; (*b*) $Ca = 2.0$ at $t = 0, 2, 4, 6, 8, 10$.

In figure 7 we consider the case of a larger drop with $a = 1.2$ and $\lambda = 0.1$. In figure 7(*a*) we set $Ca = 1.0$ while in figure 7(*b*) we set $Ca = 2.0$. Note that for $Ca = 1.0$ the drop evolves into a steady state and a small indentation develops on the trailing end whereas the smaller drop in figure 6 with $a = 0.9$ had the jetting behaviour. In figure

7(*b*) we again find the jetting behaviour but at the larger capillary number of $Ca = 2.0$. Here the outer fluid penetrates the entire length of the original drop before the end of the tail closes up. Thus increasing the volume of the drop has also raised the critical capillary number at which we lose the stability of the steady states observed in figure 7(*a*). Olbricht & Kung (1992) found that for effective radii greater than 0.95, the critical Ca tends to a constant value. This was not observed for the cases we have considered but may be possible at larger values of a. We should also note that a jetting behaviour was also observed in the computations of Pozrikidis (1992) for a periodic array of drops with a less than 1 for small and zero inverse Bond number (i.e. large and infinite Ca in our scaling). When jetting occurred with $a > 1$ his calculations were strongly influenced by the periodicity.

6. Constricted capillary

The problem of a drop flowing in a constricted capillary is now considered. The constriction is given by (2.15). For our initial series of runs we set $l = 1$ and $d = 0.3$. Hence the radius of the tube at its narrowest part is $1-2d = 0.4$. We note that by conservation of mass, the fluid velocity increases like $1/(1-2d)^2$ as it flows through the constriction. Therefore, as the constriction depth increases, the velocity in the constriction would also increase, and we can expect that the solution will become more difficult to compute because of the large velocity gradients. In the computations, the front of the bubble at $t = 0$ is always placed at $z = -(l+0.1)$ on the upstream side of the constriction.

In figure 8(*a*) we show the evolution of an initially spherical bubble moving through a constriction with $a = 0.9$, $\lambda = 0.001$ and $Ca = 0.1$. Because of the small viscosity ratio, we refer to this case as a bubble moving in a constriction. Note that after a portion of the nose passes the neck of the constriction, the sides of the bubble begin to come in, leading to a snap-off, i.e. a portion of the bubble breaks off to form a separate bubble. We say that the bubble has snapped off when the radial coordinate is less than 0.02 at the point where snap-off occurs. This is a reasonable criterion for snap-off since any additional decrease in the neck radius happens very quickly and further computations of the solution become difficult because of the large velocity gradients in the neighbourhood of the snap-off. It is clear from figure 8 that the snap-off point is not located at the centre of the constriction but at the downstream of the neck. Also, a closer inspection of the bubble surface velocities indicates that for this case there is no backflow at the downstream side of the constriction up to the time calculated. In this case, a new bubble is generated by the flush of suspending fluid flowing down the constriction from upstream. In figure 8(*b*) we plot the jump in pressure ΔP across the constricted capillary as a function of time. Here we define $\Delta P = p(z=-6) - p(z=6)$. It shows that a slight increase in the pressure jump is required in order to push the bubble through the constriction. Once the front of the bubble passes through the centre of the constriction, the pressure jump drops sharply and then continues to decrease slightly as more of the bubble moves through the constriction. Then as snap-off is occurring, the pressure jump increases.

Suppose we now vary Ca and keep all the other parameters fixed. Previous studies have pointed out the importance of Ca in determining the bubble speed and the thickness of the film left between the bubble and the tube wall. We find that as the bubble moves through the constriction each of these effects strongly influences whether or not snap-off will occur. Figure 9 shows the evolution of the same bubble as in figure 8 but with different values of Ca. In figure 9(*a*) we set $Ca = 0.05$. Note that the film

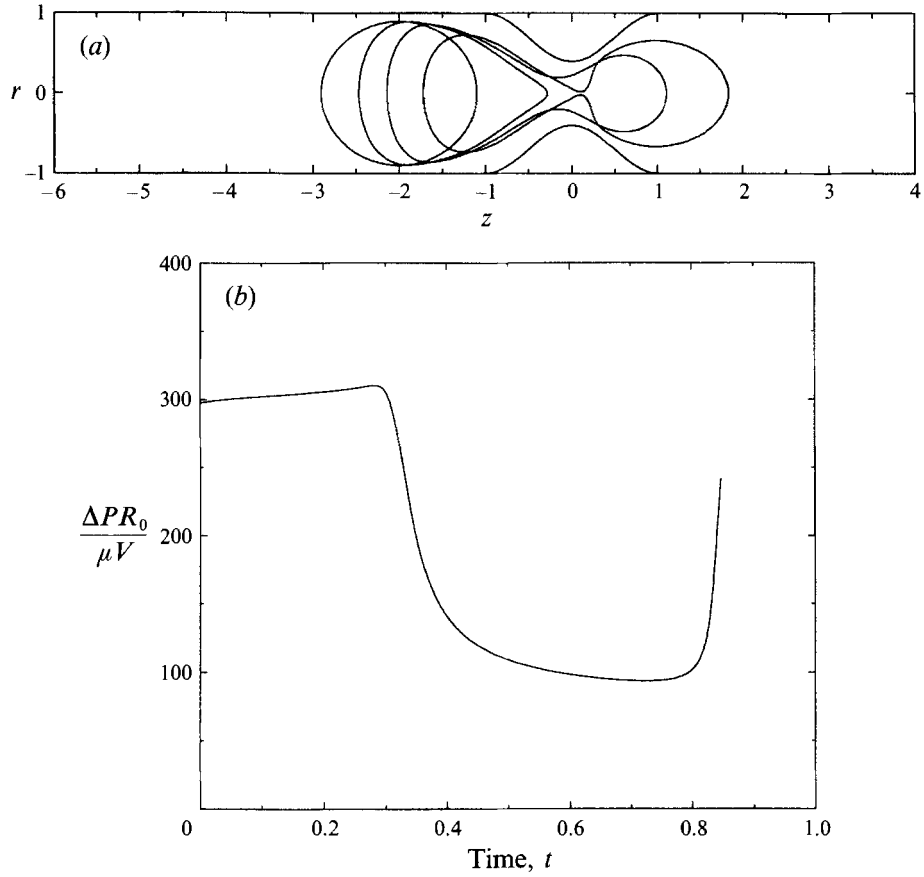

FIGURE 8. (*a*) Evolution of an initially spherical bubble with $a = 0.9$, $\lambda = 0.001$ and $Ca = 0.1$ at $t = 0$, 0.25, 0.5, 0.85. (*b*) Pressure jump across the constricted capillary as a function of time for an initially spherical bubble with $a = 0.9$, $\lambda = 0.001$ and $Ca = 0.1$.

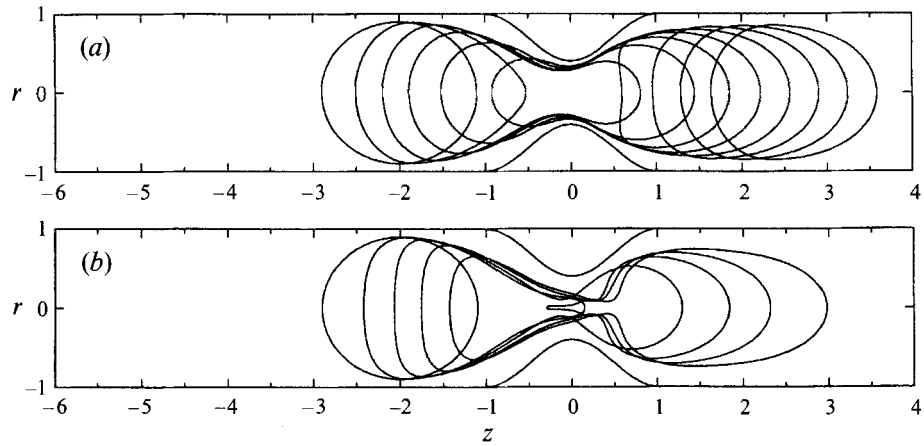

FIGURE 9. Evolution of an initially spherical bubble with $a = 0.9$, $\lambda = 0.001$: (*a*) $Ca = 0.05$ at $t = 0$, 0.25, 0.5,..., 2.25; (*b*) $Ca = 0.2$ at $t = 0$, 0.25, 0.5, 0.75, 1.0, 1.36.

left between the bubble and the tube wall is clearly thinner than for $Ca = 0.1$. Consequently, there is less fluid in the neighbourhood of the neck and so the instability associated with the growth of the coating film takes longer to develop (see e.g. Gauglitz & Radke 1990). Hence the bubble passes through the constriction and attains a steady shape at the downstream side of the constriction. On the other hand, for $Ca = 0.2$, the thickness of the film left between the bubble and the tube wall is comparable to that for $Ca = 0.1$. Although the film is thick enough to drive the fluid into the constriction from upstream and allow the snap-off instability to grow, the velocity of the bubble is so fast that it moves out of the constriction before the instability can grow significantly. We note that as the bubble passes through the constriction, a thread of fluid at the rear of the bubble is observed. We expect this thread of fluid to be unstable and to break up into pieces. The phenomenon is difficult to capture accurately with our numerical method because of the thinness of the thread, so we do not follow it to breakup. Also, because of the thinness of the thread, this instability is closely related to the pinch-off instability discussed in §4, so we distinguish between the thread breaking up and the snap-off of figure 8. Hence for $Ca = 0.2$ most of the bubble goes through the constriction owing to the high velocity of the suspending fluid and leaves a thread at its tail which would break into pieces. We have also found this thread of fluid at higher capillary numbers.

The above calculations imply that for a bubble with finite volume, there is a range of capillary numbers at which a given bubble will snap off. This should be contrasted with the observations of Gauglitz & Radke (1990) who considered the motion of an infinite film and a semi-infinite bubble (Gauglitz 1986) in a constricted capillary using a lubrication model at low capillary number. They estimate (their equation (23)), for a fixed geometry, that the ratio of the travel time for a bubble to move through the constriction to the response time of the interface to grow is proportional to the capillary number (their capillary number is defined in terms of the velocity of the bubble front not the flux, and by bubble they were referring to the front of their semi-infinite bubble). We can reinterpret travel time here as the time for a finite bubble to pass through the constriction if we make this ratio proportional to the capillary number times the ratio of the steady bubble length to the constriction length. Hence a given bubble is not expected to snap off at small capillary numbers. But if the capillary number is large, we would expect to see snap-off since the interface instability grows faster. Our results are consistent with the first prediction but not the second one, the most likely reason being that their estimates are for a small capillary number in the lubrication limit and also the results in figures 8 and 9 are for finite bubbles.

So far we have considered the impulsive motion of an initially spherical bubble moving through the constriction. Suppose we use the steady-state profiles computed in §5 as initial data and keep the same parameters as in figures 8 and 9. The effect of changing these initial data is illustrated in figure 10 which shows the evolution of an initial steady-shape bubble passing through the constriction. Note that the initial steady shape also depends on Ca. We find that the overall dynamics are similar to the initially spherical bubble. However, for $Ca = 0.1$ where snap-off occurs, the snap-off time, τ, defined by the difference between the time when the bubble front passes the centre of the constriction and the time snap-off occurs, is shorter for the steady-shape bubble ($\tau = 0.43$) than for the spherical bubble ($\tau = 0.56$). Hence the bubble generated by the initially steady-shape profile after snap-off has a smaller effective radius ($b_r = 0.65$) than the spherical bubble case ($b_r = 0.72$).

We now study the effect of bubble size by increasing the effective radius a. In figure 11, we show the evolution of an initially steady-shape bubble with $a = 1.2$. The other

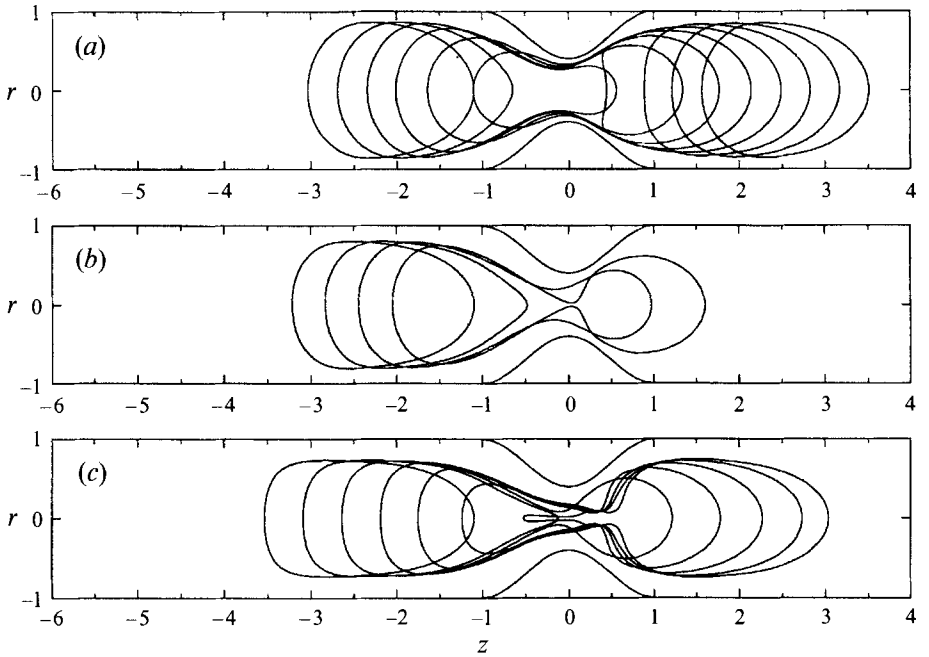

FIGURE 10. Evolution of an initially steady shape bubble with $a = 0.9$, $\lambda = 0.001$: (*a*) $Ca = 0.05$ at $t = 0, 0.25, 0.5, \ldots, 2.25$; (*b*) $Ca = 0.1$ at $t = 0, 0.25, 0.5, 0.76$; (*c*) $Ca = 0.2$ at $t = 0, 0.25, 0.5, \ldots, 1.25$, and $t = 1.42$.

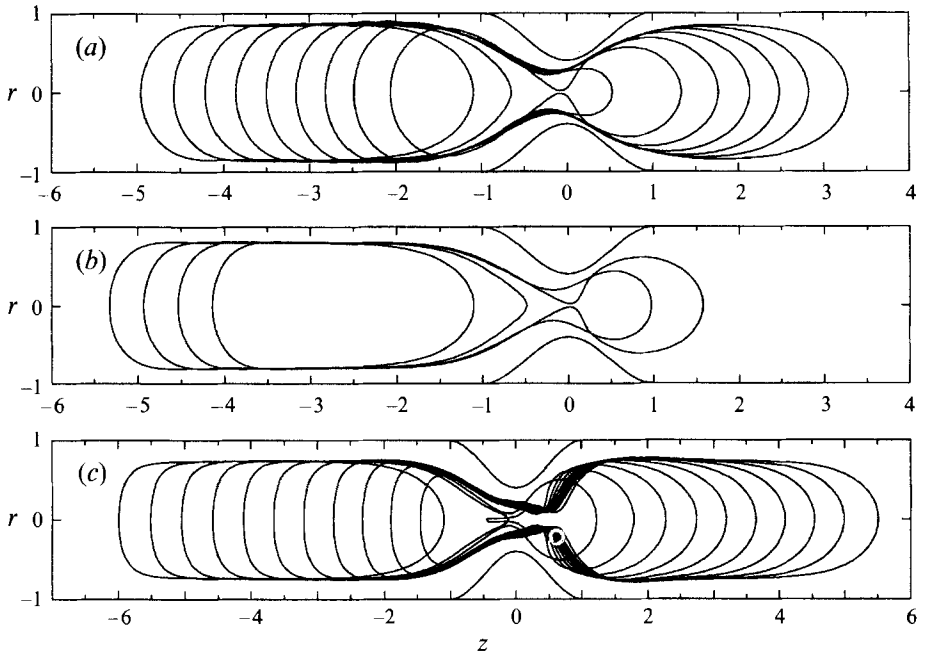

FIGURE 11. Evolution of an initially steady-shape bubble with $a = 1.2$, $\lambda = 0.001$: (*a*) $Ca = 0.05$ at $t = 0, 0.25, 0.5, \ldots, 1.75$, and $t = 2.09$; (*b*) $Ca = 0.1$ at $t = 0, 0.25, 0.5, 0.75$; (*c*) $Ca = 0.2$ at $t = 0, 0.25, 0.5, \ldots, 2.5$, and $t = 2.79$.

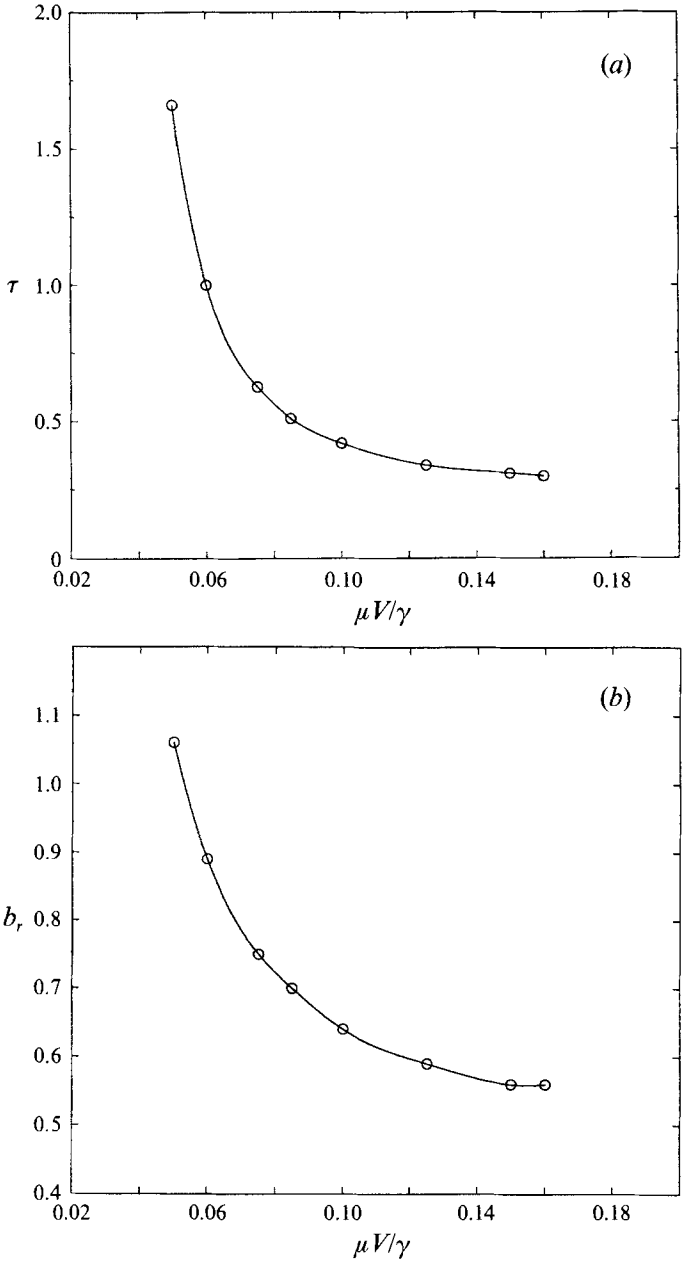

FIGURE 12. (*a*) Snap-off time τ as a function of capillary number for $a = 1.2$ and $\lambda = 10^{-3}$. (*b*) The effective radius of the bubble generated, b_r, as a function of capillary number for $a = 1.2$ and $\lambda = 10^{-3}$.

parameters are the same as in figure 10. We now see that both the $Ca = 0.05$ and $Ca = 0.1$ cases snap off. The snap-off times and the effective radius of the bubble generated are $\tau = 1.66$ and $b_r = 1.06$ for $Ca = 0.05$, and $\tau = 0.42$ and $b_r = 0.64$ for $Ca = 0.1$. Hence we see that for $Ca = 0.1$, τ and b_r are slightly smaller than for the smaller bubble case of $a = 0.9$. The fact that the $Ca = 0.05$ case now snaps implies that the longer bubble allows extra time for the instability to grow and, in contrast to $Ca = 0.1$,

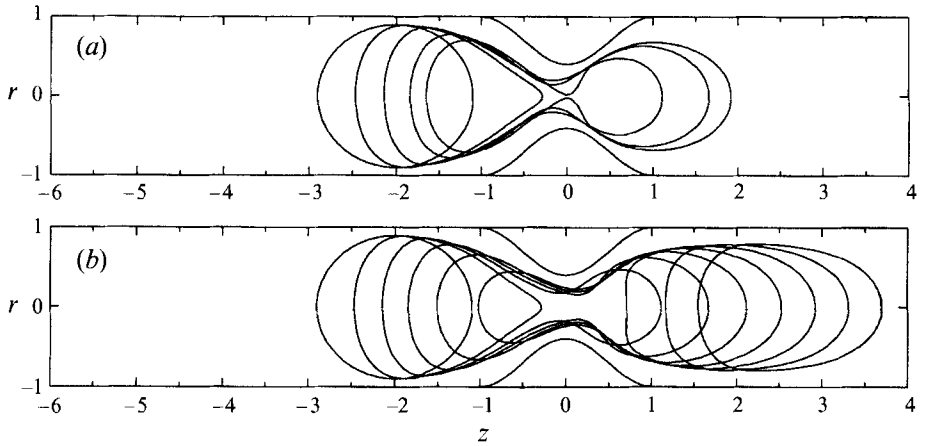

FIGURE 13. Evolution of an initially spherical bubble with $a = 0.9$, $Ca = 0.1$: (*a*) $\lambda = 0.0005$ at $t = 0, 0.25, 0.5, 0.75, 0.90$; (*b*) $\lambda = 0.01$ at $t = 0, 0.25, 0.5, \ldots, 2$.

a weak backflow occurs at the downstream side of the constriction. The $Ca = 0.2$ profiles are very similar for both the $a = 0.9$ and $a = 1.2$ cases: both have a thread of fluid at the rear after most of the bubble has passed through the neck. Figure 12 shows the snap-off time, τ, and the effective radius of the generated bubble, b_r, as a function of Ca for $a = 1.2$ and $\lambda = 10^{-3}$. We have found snap-off for Ca between 0.05 and 0.16 corresponding to $b_r = 1.06$ and 0.56, respectively. For smaller capillary number, e.g. $Ca = 0.03$, we have not observed snap-off behaviour. Selective runs for $a = 1.4$ indicate the same values of τ and b_r for $Ca = 0.1$ and higher. However, for $Ca = 0.05$, the value of b_r is slightly larger.

The dependence of the bubble dynamics on the viscosity ratio is shown in figure 13. In figure 13(*a*) we set $\lambda = 0.0005$ and in figure 13(*b*) we set $\lambda = 0.01$; the other parameters are the same as in figure 8. We find that the $\lambda = 0.0005$ case snaps while the $\lambda = 0.01$ case does not. For the $\lambda = 0.001$ case of figure 8, we find that $\tau = 0.56$ and $b_r = 0.72$, while for the $\lambda = 0.0005$ case $\tau = 0.60$ and $b_r = 0.74$. Hence decreasing λ increases the snap-off time and the size of the bubble generated. These results illustrate the sensitivity of the snap-off mechanism to λ. The dynamics for different values of λ are revealed with an inspection of the surface velocity. After the bubble front passes through the neck and before snap-off can occur, the velocity of the suspending fluid flowing down the constriction increases with λ (since viscous drops are harder to deform and can support higher velocity). This means that the potential snap-off points for $\lambda = 0.0005$ move slower than for $\lambda = 0.001$. However, the bubble speed at the front is relatively independent of these small values of λ. So the snap-off time is longer for the smaller λ and a larger bubble is generated. For $\lambda = 0.01$, the potential snap-off points are swept away to the right side of the constriction by the high velocity so no snap-off can occur. We note that in our numerical studies we have only considered values of λ bounded away from zero, because the numerical error increases significantly with decreasing λ. Similar difficulties have been observed by previous researchers, e.g. see Tjahjadi, Stone & Ottino (1992). Hence in order to control this error the runs in this section have been mostly done for $\lambda = 10^{-3}$.

The parameters studied so far are all physical parameters. We now consider the effects of geometric parameters, namely the parameters d and l, which determine the depth and the length of the constriction with the same physical parameters as in figure 11(*b*).

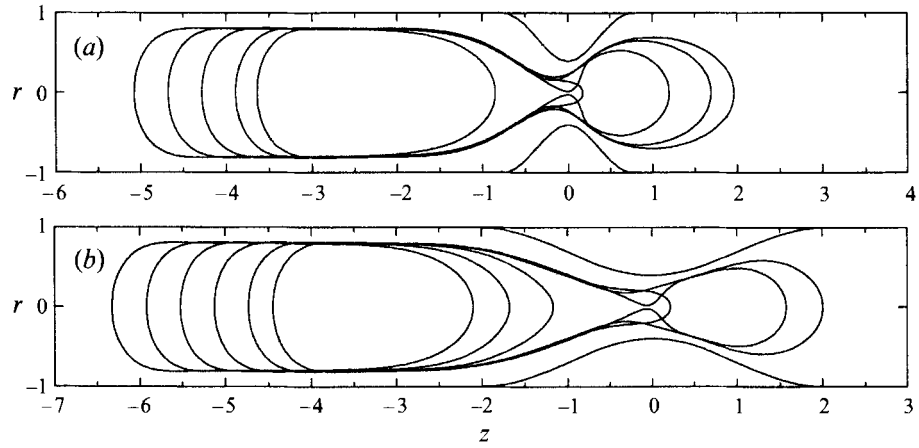

FIGURE 14. Evolution of an initially steady shape bubble with $a = 1.2$, $\lambda = 0.001$ and $Ca = 0.1$: (*a*) $l = 0.75$ at $t = 0$, 0.25, 0.5, 0.75, 0.91; (*b*) $l = 2.0$ at $t = 0$, 0.25, 0.5, ..., 1.0, and $t = 1.18$.

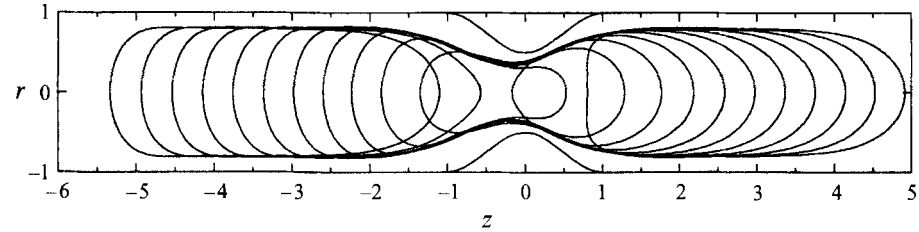

FIGURE 15. Evolution of an initially steady shape bubble with $a = 1.2$, $\lambda = 0.001$, $Ca = 0.1$ and $d = 0.25$ at $t = 0$, 0.25, 0.5, ..., 3.0.

Figure 14 shows the evolution of an initially steady-shape bubble moving through constrictions of different lengths. In figure 14(*a*) we set $l = 0.75$ and find that snap-off occurs with $\tau = 0.68$ and $b_r = 0.77$. In figure 14(*b*) we set $l = 2.0$ and observe that snap-off occurs with $\tau = 0.45$ and $b_r = 0.68$. Hence the snapped off bubble in this slowly varying constriction is slightly larger than the $l = 1.0$ case, but a slightly sharper constriction results in a longer snap-off time and a larger bubble. This implies that the dynamics is strongly dependent on the shape of the constriction. Also we note that the snap-off point occurs to the left of the neck for $l = 2.0$. This upstream snap-off was also observed in the lubrication model of Gauglitz (1986) who assumed a slowly varying constriction. In figure 15 we set $d = 0.25$. Hence the constriction is not as deep and we see that snap-off no longer occurs. So a critical depth of the constriction is also required for snap-off to occur.

7. Conclusions

The pressure-driven motion of a bubble (or drop) through a capillary tube has been studied here. The solutions were determined by solving the Stokes equations numerically with a boundary integral method. Solutions for both a straight and a constricted capillary tube were determined.

In the straight-tube case we were able to determine steady-state solutions for a given finite bubble as long as the capillary number was small enough. For larger capillary numbers, we found that as we marched in time, the drop elongated and a jet of

suspending fluid entered the drop from the back. This behaviour is also typical of what has been observed experimentally.

In a constricted tube we found that if the viscosity ratio was too large, then a bubble (or drop) passes through a given constriction. For small viscosity ratio, it is possible to select a range of parameters for which a given finite bubble will snap off as it passes through a constriction. For the finite bubbles considered in this study, if the capillary number was too large or too small the snap-off instability would not occur. In the results presented here, only values of the parameters were selected at which a steady-state solution of the bubble existed in a straight tube. We should note that the jetting instability occurring in a straight tube can also occur as a bubble or drop passes a constriction. Hence, it is possible for a drop to pass through a constriction and initiate a jetting instability. After the drop passes through the constriction, if a steady-state solution exists, then the drop will evolve to it. These results have been observed numerically by Miksis & Tsai (1993).

This research was supported in part by Department of Energy grant DE-FG02-88ER13927.

REFERENCES

BRENNER, H. 1971 Pressure drop due to the motion of neutrally buoyant particles in duct flows. II. Spherical droplets and bubbles. *Indust. Engng Chem. Fund.* **10**, 537–543.

BORHAN, A. & MAO, C. F. 1992 Effect of surfactants on the motion of drops through circular tubes. *Phys. Fluids* **4**, 2628–2640.

BRETHERTON, F. P. 1961 The motion of long bubbles in tubes. *J. Fluid Mech.* **10**, 166–188.

CHI, B. K. & LEAL, L. G. 1989 A theoretical study of the motion of a viscous drop toward a fluid interface at low Reynolds number. *J. Fluid Mech.* **201**, 123–146.

GAUGLITZ, P. A. 1986 Instability of liquid films in constricted capillaries: A pore level description of foam generation in porous media. PhD thesis, University of California, Berkeley, California.

GAUGLITZ, P. A. & RADKE, C. J. 1990 The dynamics of liquid film breakup in constricted cylindrical capillaries. *J. Colloid Interface Sci.* **134**, 14–40.

GAUGLITZ, P. A., ST. LAURENT, C. M. & RADKE, C. J. 1988 Experimental determination of gas-bubble breakup in a constricted cylindrical capillary. *Indust. Engng Chem. Res.* **27**, 1282–1291.

GOLDSMITH, H. L. & MASON, S. G. 1963 The flow of suspensions through tubes: II. Single large bubbles. *J. Colloid Sci.* **18**, 237–261.

HAMMOND, P. S. 1983 Nonlinear adjustment of a thin annular film of viscous fluid surrounding a thread of another within a circular cylindrical pipe. *J. Fluid Mech.* **137**, 363–384.

HAPPEL, J. & BRENNER, H. 1965 *Low Reynolds Number Hydrodynamics.* Prentice-Hall.

HETSRONI, G., HABER, S. & WACHOLDER, E. 1970 The flow field in and around a droplet moving axially within a tube. *J. Fluid Mech.* **41**, 689–705.

HO, B. P. & LEAL, L. G. 1975 The creeping motion of liquid drops through a circular tube of comparable diameter. *J. Fluid Mech.* **71**, 361–384.

LADYZHENSKAYA, O. A. 1969 *The Mathematical Theory of Viscous Incompressible Flow*, 2nd edn. Gordon and Breach.

LEE, S. H. & LEAL, L. G. 1982 The motion of a sphere in the presence of a deformable interface. II. A numerical study of the translation of a sphere normal to an interface. *J. Colloid Interface Sci.* **87**, 81–106.

MARTINEZ, M. J. & UDELL, K. S. 1988 Axisymmetric creeping motion of drops through a periodically constricted tube. *AIP Conf. Proc.* **197**, 222–234.

MARTINEZ, M. J. & UDELL, K. S. 1989 Boundary integral analysis of the creeping flow of long bubbles in capillaries. *Trans. ASME* E: J. Appl. Mech. **56**, 211–217.

MARTINEZ, M. J. & UDELL, K. S. 1990 Axisymmetric creeping motion of drops through circular tubes. *J. Fluid Mech.* **210**, 565–591.

MIKSIS, M. J. & TSAI, T. M. 1993 Effects of capillarity on microscopic flow in porous media. *Proc. 11th Symp. Energy Engng Sci. at Argonne National Laboratory*, pp. 24–31.

OLBRICHT, W. L. & KUNG, D. M. 1992 The deformation and breakup of liquid drops in low Reynolds number flow through a capillary. *Phys. Fluids* **4**, 1347–1354.

OLBRICHT, W. L. & LEAL, L. G. 1983 The creeping motion of immiscible drops through a converging/diverging tube. *J. Fluid Mech.* **134**, 329–355.

POZRIKIDIS, C. 1991 *Boundary Integral and Singularity Methods for Linearized Viscous Flow.* Cambridge University Press.

POZRIKIDIS, C. 1992 The buoyancy-driven motion of a train of viscous drops within a cylindrical tube. *J. Fluid Mech.* **237**, 627–648.

RALLISON, J. M. & ACRIVOS, A. 1978 A numerical study of the deformation and burst of a viscous drop in an extensional flow. *J. Fluid Mech.* **89**, 191–200.

REINELT, D. A. & SAFFMAN, P. G. 1985 The penetration of a finger into a viscous fluid in a channel and tube. *SIAM J. Sci. Statist. Comput.* **6**, 542–561.

ROOF, J. G. 1970 Snap-off of oil droplets in water-wet pores. *Soc. Petrol. Engng J.* **10**, 85–90.

SCHWARTZ, L. W., PRINCEN, H. M. & KISS, A. D. 1986 On the motion of bubbles in capillary tubes. *J. Fluid Mech.* **172**, 259–275.

SHEN, E. I. 1984 Flow and breakup of inviscid bubbles in porous media. PhD thesis, University of California, Berkeley, California.

SHEN, E. I. & UDELL, K. S. 1985 A finite element study of low Reynolds number two-phase flow in cylindrical tube. *Trans. ASME* E: J. Appl. Mech. **52**, 253–256.

TAYLOR, G. I. 1961 Deposition of a viscous fluid on the wall of a tube. *J. Fluid Mech.* **10**, 161–165.

TJAHJADI, M., STONE, H. A. & OTTINO, J. M. 1992 Satellite and subsatellite formation in capillary breakup. *J. Fluid Mech.* **243**, 297–317.

TSAI, T. M. 1994 Numerical solutions of free surface flow with surface tension at low Reynolds number. PhD thesis, Northwestern University, Evanston, Illinois.

YOUNGREN, G. K. & ACRIVOS, A. 1976 On the shape of a gas bubble in a viscous extensional flow. *J. Fluid Mech.* **76**, 433–442.